

# Feasibility of biepitaxial $\text{YBa}_2\text{Cu}_3\text{O}_{7-x}$ Josephson junctions for fundamental studies and potential circuit implementation

F. Tafuri

*Dipartimento di Ingegneria dell'Informazione, Seconda Università di Napoli, 81031 Aversa (CE) and  
INFN-Dipartimento Scienze Fisiche dell'Università di Napoli "Federico II", 80125 Napoli (ITALY)*

F. Carillo, F. Lombardi, F. Miletto Granozio, F. Ricci, U. Scotti di Uccio and A. Barone  
*INFN-Dipartimento Scienze Fisiche dell'Università di Napoli "Federico II", 80125 Napoli (ITALY)*

G. Testa and E. Sarnelli

*Istituto di Cibernetica del CNR, Via Toiano 6, Arco Felice (NA) (ITALY) also  
INFN*

J.R. Kirtley

*IBM T.J. Watson Research Center, P.O. Box 218, Yorktown Heights, NY 10598,  
USA*

(November 10, 2018)

We present various concepts and experimental procedures to produce biepitaxial  $\text{YBa}_2\text{Cu}_3\text{O}_{7-x}$  grain boundary Josephson junctions. The device properties have an interesting phenomenology, related in part to the possible influence of “ $\pi$ -loops”. The performance of our junctions and Superconducting Quantum Interference Devices indicates significant improvement in the biepitaxial technique. Further, we propose methods for fabricating circuits in which “0-” and “ $\pi$ -loops” are controllably located on the same chip.

## I. INTRODUCTION

The possibility of realizing electronic circuits in which the phase differences of selected Josephson junctions are biased by  $\pi$  in equilibrium is quite stimulating.<sup>1</sup> The concept of such  $\pi$ -phase shifts was originally developed in the “extrinsic” case for junctions with ferromagnetic barriers<sup>2</sup> and in the “intrinsic” case for junctions exploiting superconductors with unconventional order parameter symmetries.<sup>3</sup> As a result of the possible  $d_{x^2-y^2}$  order parameter symmetry of high critical temperature superconductors (HTS),<sup>4</sup> the presence of intrinsic  $\pi$  loops has also been considered for HTS systems.<sup>5</sup> This has been discussed recently in view of novel device concepts, and in particular for the implementation of a solid state qubit<sup>1,6-8</sup> and for Complementary Josephson junction electronics.<sup>9</sup> In this paper we discuss how  $\text{YBa}_2\text{Cu}_3\text{O}_{7-x}$  (YBCO) structures made by the biepitaxial technique<sup>10,11</sup> can be successfully employed to produce arbitrary circuit geometries in which both “0” and  $\pi$ -loops are present, and possibly to obtain a doubly degenerate state.<sup>1,6</sup> Of course, great caution should be used because of stringent requirements on junctions parameters for practical applications of such devices.

Josephson junctions based on artificially controlled grain boundaries have been widely employed for fundamental studies on the nature of HTS.<sup>4,7,8</sup> The lack of a

reliable technology based on the traditional trilayer configuration (i.e. a sandwich type junction with an insulator between the two superconducting electrodes) also enhanced interest in GB Josephson junctions for applications. Although the mechanism of high- $T_C$  superconductivity and the influence of grain boundaries on the transport properties are not completely determined, reproducible and good quality devices are routinely fabricated. YBCO GB junctions are usually classified as bicrystals,<sup>12</sup> biepitaxials,<sup>11</sup> and step-edges,<sup>13</sup> depending on the fabrication procedure. The bicrystal technique typically offers junctions with better performances and allows in principle the realization of all different types of GBs ranging from [001] and [100] tilt to [100] twist boundaries. GB junctions based on the step-edge and biepitaxial techniques offer the advantage, with respect to the bicrystal technology, of placing the junctions on the substrate without imposing any restrictions on the geometry. A comparison between the different GB techniques is far beyond the aim of this paper. Nevertheless we intend to show that significant improvements with respect to the original technique developed by Char et al.<sup>11</sup> are possible for biepitaxial junctions, and that the resulting devices have potential for applications. As a matter of fact, in traditional biepitaxial junctions, the seed layer used to modify the YBCO crystal orientation on part of the substrate produces an artificial  $45^\circ$  [001] tilt (c-axis

tilt) GB. The nature of such a GB seems to be an intrinsic limit for some real applications. A convincing explanation has been given in terms of the d-wave nature of the order parameter and more specifically by the presence of  $\pi$ -loops.<sup>14</sup> As demonstrated by studies on bicrystals, based on the same type of 45° [001] tilt GB, the presence of  $\pi$ -loops reduces the  $I_C R_N$  values (where  $I_C$  and  $R_N$  are the critical current and the high normal state resistance respectively), produces a dependence of the critical current  $I_C$  on the magnetic field  $H$  quite different from the Fraunhofer-like pattern, and generates unquantized flux noise at the grain boundary.<sup>14</sup>

We will show that the implementation of the biepitaxial technique<sup>10</sup> we developed to obtain 45° [100] tilt and twist (a-axis tilt and twist) GBs junctions makes such a technique interesting for both applications and fundamental studies. The phenomenology observed for the junctions based on these GBs and Scanning SQUID Microscopy investigations demonstrate the absence of  $\pi$ -loops, as we expect from their microstructure. As a consequence higher values of the  $I_C R_N$  values, a Fraunhofer like dependence of  $I_C$  on the magnetic field and lower values of the low frequency flux noise, when compared with 45° c-axis tilt GBs, have been measured. These features are important tests to employ junctions for applications. Scanning SQUID Microscopy investigations also gave evidence of “fractional” vortices in the presence of impurities. Finally, we extended the biepitaxial process to other types of GB by using different seed layers to obtain junction configurations where  $\pi$  loops can be controllably produced. We shall not dwell on conceptual principles and actual feasibility of qubit devices. Instead we discuss the importance of the biepitaxial technique in having “0” and “ $\pi$ ” loops on the same chip. This makes the biepitaxial technique more versatile and promising for circuit design.

## II. DEVICES: CONCEPTS AND FABRICATION PROCEDURE

As mentioned above, the biepitaxial technique allows the fabrication of various GBs by growing different seed layers and using substrates with different orientations. We have used MgO, CeO<sub>2</sub> and SrTiO<sub>3</sub> as seed layers. The MgO and CeO<sub>2</sub> layers are deposited on (110) SrTiO<sub>3</sub> substrates, while SrTiO<sub>3</sub> layers are deposited on (110) MgO substrates; in all these cases the seed layers grow along the [110] direction. Ion milling is used to define the required geometry of the seed layer and of the YBCO thin film respectively, by means of photoresist masks. YBCO films, typically 120nm in thickness, are deposited by inverted cylindrical magnetron sputtering at a temperature of 780° C. YBCO grows along the [001] direction on MgO (substrates or seed layers) and on the CeO<sub>2</sub> (seed layers), while it grows along the [103]/[013] direction on SrTiO<sub>3</sub> (substrates or seed layers). In order to select the [103] or  $\bar{1}03$  growth and to ensure a better structural uniformity

of the GB interface, we have also successfully employed vicinal substrates. However, most of the transport properties presented in this paper refer to samples not using vicinal substrates. Detailed structural investigations on these GBs, including Transmission Electron Microscopy (TEM) analyses, have been performed and the results have been presented elsewhere.<sup>10,16</sup>

Depending on the patterning of the seed layer and the YBCO thin film, different types of GBs ranging from the two ideal limiting cases of 45° a-axis tilt and 45° a-axis twist have been obtained (see Fig.1). The intermediate situation occurs when the junction interface is tilted at an angle  $\alpha$  different from 0 or  $\pi/2$  with respect to the a- or b-axis of the [001] YBCO thin film. In all cases, the order parameter orientations do not produce an additional  $\pi$  phase shift along our junction, in contrast with the 45° asymmetric [001] tilt junctions. As a consequence, no  $\pi$  loops should occur independently of the details of the interface orientation. In Fig. 1 we consider ideal interfaces and neglect meandering of the GBs or interface anomalies that will be considered below. The CeO<sub>2</sub> seed layer may produce a more complicated GB structure, in which a 45° c-axis tilt accompanies the 45° a-axis tilt or twist (see Fig.2a).<sup>15</sup> In this case, as shown in Fig.2b,  $\pi$  loops should occur in analogy with the traditional biepitaxial junctions based on 45° c-axis tilt GBs. In both Figs. 1 and 2 we display the possible  $d_{x^2-y^2}$  -wave order parameter symmetry in the junction configuration. Junctions were typically 4 microns wide. We also performed systematic measurements on SQUIDs based on the structure employing MgO as a seed layer and SrTiO<sub>3</sub> as a substrate. DC SQUIDs in different configurations and with loop inductance typically ranging from 10 to 100 pH have been investigated. The typical loop size leading to the 10(100) pH inductance is approximately  $10^2 \mu\text{m}^2$  ( $10^4 \mu\text{m}^2$ ).

## III. EXPERIMENTAL RESULTS

### A. Biepitaxial junctions employing MgO seed layers

In this section we attempt to cover most of the phenomenology of the transport properties of 45° a-axis tilt and twist biepitaxial junctions. In Fig. 3, current vs voltage (I-V) characteristics of a typical biepitaxial junction are given for various temperatures close to the critical temperature. In the inset the corresponding I-V characteristic at  $T = 4.2$  K is reported. They are closely described by the resistively-shunted-junction (RSJ) model and no excess current is observed. Nominal critical current densities  $J_C$  of  $5 \times 10^2 \text{A/cm}^2$  at  $T = 77$  K, and of  $9 \times 10^3 \text{A/cm}^2$  at  $T = 4.2$  K have been measured respectively. The  $R_N$  value ( $3.2 \Omega$ ) is roughly independent of the temperature for  $T < T_C$ , providing a normal state specific conductance  $\sigma_N = 70 (\mu\Omega\text{cm}^2)^{-1}$ . The maximum working temperature  $T_C$  of this device was 82 K. In this case

$I_C R_N$  is 1.3 mV at  $T = 4.2$  K. These values typically ranged from 1 mV to 2 mV at  $T = 4.2$  K. They are larger for the corresponding  $J_C$  values than those provided by conventional biepitaxials, and are of the same order of magnitude as in GB bicrystal and step edge junctions.<sup>10</sup> While the values of critical current density and normal state specific conductance in the tilt case are quite different from the twist case, the  $I_C R_N$  values are approximately the same for both. Moreover  $I_C R_N$  does not scale with the critical current density.<sup>10</sup> In the tilt cases  $J_C \approx 0.5\text{-}10 \cdot 10^3$  A/cm<sup>2</sup> and  $\sigma_N \approx 1\text{-}10$  ( $\mu\Omega\text{cm}^2$ )<sup>-1</sup> are measured at  $T = 4.2$  K respectively. Twist GBs junctions are typically characterized by higher values of  $J_C$  in the range  $0.1\text{-}4.0 \cdot 10^5$  A/cm<sup>2</sup> and of  $\sigma_N$  in the range 20-120 ( $\mu\Omega\text{cm}^2$ )<sup>-1</sup> (at  $T = 4.2$  K). For the twist case deviations from the RSJ model are more marked as a result of higher critical current densities. For high values of  $J_C$  GB junctions do not present any clear modulation of the critical current as a function of the magnetic field.

A demonstration of the possibility of tailoring the critical current density and of the different transport regimes occurring in the tilt and twist cases has been given by measuring the properties of junctions with different orientations of the GB barrier on the same chip. By patterning the seed layer as shown in Fig.4a, we could measure the properties of a tilt junction and of junctions whose interface is tilted in plane by an angle  $\alpha = 30^\circ, 45^\circ$  and  $60^\circ$  with respect to the a- or b-axis of the [001] YBCO thin film respectively. In all cases the order parameter orientations do not produce an additional  $\pi$  phase shift along our junction, in contrast with the  $45^\circ$  [001] tilt junctions, and no  $\pi$  loops should occur. We measured the expected increase of the critical current density with increasing angle, which corresponds on average to an increase of the twist current component. The values measured at  $T = 4.2$  K are reported in Fig. 4a and range from the minimum value  $J_C = 3 \cdot 10^2$  A/cm<sup>2</sup> in the tilt case to the maximum  $J_C = 10^4$  A/cm<sup>2</sup> corresponding to an angle of  $60^\circ$ , for which the twist component is higher. The consistency of this result has been confirmed by the values of normal state resistances, which are higher in the tilt case and decrease with increasing  $\alpha$ . The  $I_C R_N$  values are about the same for all the junctions independently of the angle  $\alpha$ . In Fig. 4b the I-V characteristics measured at  $T = 4.2$  K, corresponding to the junctions of Fig.4a, are shown for approximately the same voltage range. Deviations from RSJ behavior appear for higher values of the critical current density ( $\alpha = 60^\circ$ ). These results demonstrate that the grain boundary acts as a tunable barrier. This possibility of modifying the GB macroscopic interface plane by controlling the orientation of the seed layer's edge is somehow equivalent to the degree of freedom offered by bicrystal technology to create symmetric or asymmetric GBs, with the advantage of placing all the junctions on the same substrate. The  $45^\circ$  a-axis tilt and twist GBs and the intermediate situations can represent ideal structures to investigate the junction physics in a wide range of configurations. The anisotropy of the (103)

films and the possibility to select the orientation of the junction interface by suitably patterning the seed layer, and eventually the use of other seed layers which produce different YBCO in plane orientations, allow the fabrication of different types of junctions and the investigation of different aspects of HTS junction phenomenology. In particular we refer to the possibility of changing the tunneling matrix elements (by selecting the angle  $\alpha$ ) and to use the anisotropy of the layered structure of YBCO properties and of the order parameter symmetry.

The study of the junction properties in the presence of an external magnetic field  $H$  is a fundamental tool for the investigation of the Josephson effect in the various junctions, as well as a test of junction quality.<sup>17</sup> We observe modulations of the critical current  $I_C$  following the usual Fraunhofer-like dependence. The  $I_C(H)$  patterns are mostly symmetric around zero magnetic field, and in all samples the absolute maximum of  $I_C$  occurs at  $H=0$ . The presence of the current maximum at zero magnetic field is consistent with the fact that in our junction configuration the order parameter orientations do not produce an additional  $\pi$  phase shift, in contrast with the  $45^\circ$  [001] tilt GB junctions.<sup>14,10</sup> Some examples are given in Fig. 5, where the magnetic pattern relative to a SQUID and a single junction at  $T = 4.2$  K are shown respectively. In the former case we can also distinguish a smaller field modulation (with a period of 8 mG) which corresponds to the SQUID modulation (inset a). In the latter case the I-V characteristics are reported for different magnetic fields (inset b). Despite the Fraunhofer-like dependence, some deviations are evident, in agreement with most of the data available in literature.

For sake of completeness we also acknowledge some work we carried out by investigating Fiske steps as a function of  $H$  in other junctions, giving some evidence of a dielectric-like behavior<sup>18</sup> of some of the layers at the junction interface. We already reported about this work elsewhere.<sup>19</sup> The Fiske steps do not depend on the use of a particular substrate, since they have been observed in junctions based both on SrTiO<sub>3</sub> and MgO substrates. Typical values of the ratio between the barrier thickness  $t$  and the relative dielectric constant  $\epsilon_r$  range from 0.2 nm to 0.7 nm. Considerations on the dependence of  $I_C$  on the temperature ( $T$ ) can be also found in Ref.<sup>19</sup>. In junctions characterized by lower critical current densities,  $I_C$  tends to saturate at low temperatures, in contrast to those characterized by higher critical currents, for which there is a linear increase.<sup>10,20</sup>

## B. Scanning SQUID microscopy on biepitaxial junctions with MgO seed layer

Figure 6 is a scanning SQUID microscope<sup>21</sup> image of a  $200 \times 200 \mu\text{m}^2$  area along a grain boundary separating a (100) region from a (103) region (as labelled in the figure) of a thin YBCO biepitaxial film grown as described

above. The position of the grain boundary is indicated by the dashed line. The image was taken at 4.2K in liquid helium with an octagonal SQUID pickup loop 4 microns in diameter after cooling the sample in a few tenths of a  $\mu\text{T}$  externally applied magnetic field normal to the plane of the sample. The grey-scaling in the image corresponds to a total variation of  $0.13\Phi_0$  of flux through the SQUID pickup loop. Visible in this image are elongated inter-layer Josephson vortices in the (103) area to the right, and “fractional” vortices in the (100) area to the left, of the grain boundary. Fits to the interlayer vortices give a value for the  $c$ -axis penetration depth of about  $4\mu\text{m}$ . The “fractional” vortices are spontaneously generated in the (100) film, regardless of the value of external field applied.<sup>22</sup> Temperature dependent scanning SQUID microscope imaging shows that this spontaneous magnetization, which appears to be associated with defects in the film, arises when the film becomes superconducting.<sup>4,23</sup> Although it is difficult to assign precise values of total flux to the “fractional” vortices, since they are not well separated from each other, fits imply that they have less than  $\Phi_0$  of total flux in them, an indication of broken time-reversal symmetry. Although there is apparently some flux generated in the grain boundary region, the fact that these SQUIDs have relatively low noise seems to indicate that this flux is well pinned at the temperatures at which the noise measurements were made. These results are consistent with the absence of  $\pi$  loops along the grain boundary.

### C. Biepitaxial junctions employing $\text{CeO}_2$ seed layers

The  $\text{CeO}_2$  seed layer, as anticipated in section II, may produce an artificial GB that can be seen as a result of two rotations: a  $45^\circ$  [100] tilt or twist followed by a  $45^\circ$  [001] tilt around the  $c$ -axis of the (001) film. For this junction configuration a d-wave order parameter symmetry would produce  $\pi$ -loops, as shown in Fig. 2. We notice that such  $\pi$ -loops are structurally different from those usually obtained by the  $45^\circ$  [001] tilt GB junctions based on the traditional biepitaxial and bicrystal techniques. Due to the microstructure we expect especially in the [100] tilt case low critical current densities and high normal state resistances. We found that the deposition conditions to select the uniform growth of YBCO  $45^\circ$  tilted around the  $c$ -axis of the (001) film are critical. Preliminary measurements realized on tilt-type junctions with a  $\text{CeO}_2$  seed layer gave evidence of Josephson coupling in these GBs. The measured  $I_C R_N$  values are from  $200\mu\text{V}$  to  $750\mu\text{V}$  and are in the typical range of the GBs Josephson junctions.

### D. Biepitaxial SQUIDs employing $\text{MgO}$ seed layers

In this section we report on the characterization of dc-SQUIDs which are to our knowledge the first employing the GBs discussed above.<sup>24</sup> These SQUIDs exhibit very good properties, and noise levels which are among the lowest ever reported for biepitaxial junctions.<sup>24</sup> Apart from implications for applications, these performances are important for the study of the transport properties of HTS Josephson junctions. In Fig. 7 we show the magnetic field dependence of the voltage at 77 K for different values of the bias current for a dc-SQUID with an inductance of 13 pH. At this temperature  $I_C R_N$  is about  $20\mu\text{V}$ . The corresponding value of the screening parameter  $\beta=2LI_C/\Phi_0$  is 0.03. In general low  $\beta$  values are mandatory to avoid the influence of asymmetric inductances in SQUID properties, and this has been crucial for experiments designed to study the order parameter symmetry.<sup>7</sup> The presented curves are quite typical. These SQUIDs usually work in a wide temperature range from low temperatures (4.2 K) up to temperatures above 77 K. The maximum working temperature was in this case 82 K. The achieved magnetic flux-to-voltage transfer functions  $V_\Phi = \partial V/\partial\Phi$ , where  $V$  and  $\Phi$  are the voltage across the device and the applied magnetic flux in the SQUID loop respectively, are suitable for applications. For instance at  $T = 77\text{ K}$  an experimental value of the SQUID amplitude voltage modulation  $\Delta V$  of 10.4 mV was measured, corresponding to  $V_\Phi = 36.9\mu\text{V}/\Phi_0$ .<sup>24</sup> Steps of different nature have been recurrently observed in the I-V characteristics in the washer and hole configurations and characterized also in terms of the magnetic field dependence of the voltage at different values of the bias current.

The noise spectral densities of the same dc-SQUID have been measured at  $T = 4.2\text{ K}$  and  $T = 77\text{ K}$  using standard flux-locked-loop modulated electronics. The energy resolution  $\epsilon = S_\Phi/2L$  (with  $S_\Phi$  being the magnetic-flux-noise spectral density) at  $T = 4.2\text{ K}$  and  $T = 77\text{ K}$  is reported in Fig. 8. At  $T = 4.2\text{ K}$  and 10 kHz, a value of  $S_\Phi = 3\mu\Phi_0/\sqrt{Hz}$  has been measured, corresponding to an energy resolution  $\epsilon = 1.6\times 10^{-30}\text{ J/Hz}$ . This value is the lowest reported in the literature for YBCO biepitaxial SQUIDs. Moreover, the low frequency  $1/f$  flux noise spectral density at 1 Hz is more than one order of magnitude lower than the one reported for traditional biepitaxials, as is also evident from the comparison with data at  $T = 4.2\text{ K}$  of Ref.<sup>25</sup>. The lower values of low frequency noise are consistent with the absence of  $\pi$ -loops on the scale of the faceting for these types of GBs, as clearly shown by Scanning SQUID Microscopy results. The  $\pi$ -loops produce some types of spontaneous magnetic flux in the GB region, which among other effects tends to degrade the SQUID’s noise levels.<sup>14</sup>

#### IV. BIEPITAXIAL JUNCTIONS FOR EXPERIMENTS ON THE SYMMETRY OF THE ORDER PARAMETER AND FOR A DEVELOPMENT OF CONCEPTS FOR QUBITS

The particular junction configurations investigated in this work allow some consideration of the possible impact of these types of junctions on the study of the Josephson effect and the order parameter symmetry in YBCO and on the development of concepts for devices.<sup>1,6,9,7</sup> We first recall that the biepitaxial technique can provide circuits composed completely of junctions without any  $\pi$ -loops (see Fig. 9a). By varying the interface orientation with respect to the [103] electrode orientation, the junction properties can be adjusted. On the other hand the traditional biepitaxial technique,<sup>11</sup> producing 45° [001] tilt GBs (see Fig. 9b) or the types of junctions described in the previous section by using CeO<sub>2</sub> (see Fig. 9c), can controllably generate  $\pi$ -loops on macroscopic scales. In these schemes we use a corner geometry with a 90° angle. This angle  $\alpha$  can be obviously tuned to enhance the effects related to the phase shift (see dashed line in Fig.9b) and this change is particularly easy to realize by using the biepitaxial technique.

In this section we focus our attention mainly on the feasibility of the biepitaxial junctions to obtain the doubly degenerate state required for a qubit. In Ref.<sup>1a</sup> the design is based on quenching the lowest order coupling by arranging a junction with its normal aligned with the node of the d-wave order parameter, thus producing a double periodic current-phase relation. It has been shown that the use of  $\pi$  phase shifts in a superconducting phase qubit provides a naturally bistable device and does not require external bias currents and magnetic fields.<sup>1b</sup> The direct consequence is the quietness of the device over other designs. A  $\pi$  junction provides the required doubly degenerate fundamental state, which also manifests itself in a doubly periodic function of the critical current density as a function of the phase.<sup>8</sup> The same principle has been used in small inductance five junction loop frustrated by a  $\pi$ -phase shift.<sup>1b</sup> This design provides a perfectly degenerate two-level system and offers some advantages in terms of fabrication ease and performance. HTS may represent a natural solution for the realization of the required  $\pi$ -phase shift due to the pairing symmetry of the order parameter and, therefore, due to the possibility of producing  $\pi$  phase shifts. Experimental evidence of YBCO  $\pi$ -SQUIDS has been given by employing the bicrystal technique on special tetracrystal substrates.<sup>7</sup> The biepitaxial technique, beyond providing junctions with opportune properties, would guarantee the versatility necessary for the implementation of a real device, as shown below. As a matter of fact, we notice that our technique allows the realization of circuits where  $\pi$ -loops can be controllably located in part of the substrate and separated from the rest of the circuit based on “0”-loops, i.e. junctions where no additional  $\pi$  phase

shifts arise. This can be easily made by depositing the MgO and CeO<sub>2</sub> seed layers on different parts of the substrate, which will be also partly not covered by any seed layer.

As a test to show how the biepitaxial junctions could be considered for preliminary tests and device implementation for quantum computing without the topological restriction imposed by the bicrystal technique, we refer to the structures proposed in Ref.<sup>1</sup> as exemplary circuits.

The former is composed by a s-wave (S)- d-wave (D)- s-wave (S') double junction connected with a capacitor and an ordinary “0” Josephson junction based on s-wave superconductors (the S-D'-S junction generates the doubly degenerate state). The latter consists of a five junction loop with a  $\pi$  junction. Our technique would combine the possibility of placing the ordinary “0” junctions corresponding to the MgO seed layer and to exploit the possible doubly degenerate state of asymmetric 45° GB junctions corresponding to the CeO<sub>2</sub> seed layer to replace the S-D-S' system or the  $\pi$  junction respectively. Our structure would be obviously composed only of HTS. In Figs. 10a and 10b we show how devices for instance such as those proposed in Ref.<sup>1</sup> could be obtained by employing the biepitaxial technique respectively. The application to the five junction loop is straightforward (Fig.10b) and the advantages of this structure have been already discussed in Ref.<sup>1b</sup>. The biepitaxial technique can offer possible alternatives for the realization of the structures above. In particular the double junctions of the original S-D-S' system can be also replaced by a D'-D-D" structure (Fig.10c) by exploiting our technique, in contrast to the bicrystal technology which could not give this possibility. Such a configuration could offer some advantages, if we consider that asymmetric 45° bicrystal GB Josephson junctions did not give systematic evidence of the doubly degenerate state. The doubly degenerate state seems to occur only in high quality low transparency GB junctions<sup>8,26</sup> and it is known that S-I-D junctions do not have double periodicity of the critical current as a function of the phase.<sup>26</sup> A consequence of a possible nodeless order parameter<sup>4,23</sup> at the D-D' GB interface could be a closer similarity with a S-I-D junction with loss of the doubly degenerate state. If this is the case, we speculate that the double junctions structure for symmetry reasons would produce a leading term in the Josephson coupling energy of the form  $E_d \cos 2\theta$  (double periodic) and that the possible dipolar component of the magnetic field would be almost completely compensated in this configuration.<sup>1b</sup> This can be considered as an attempt to construct a “microscopic”  $2\theta$ -junction. We finally notice that the topological advantages offered by the biepitaxial junctions would therefore be crucial in both the cases considered for the realization of the structure in Fig. 10, and important to reduce de-coherence effects. Bicrystal substrates would in fact impose on the circuit additional junctions required by the circuit design and, as a consequence, generate additional noise and de-coherence in the device.

## V. CONCLUSIONS

The performance of the presented junctions and SQUIDS demonstrates that significant improvements in the biepitaxial technique are possible, and the resulting devices have potential for applications. We have presented a phenomenology that is consistent with the expected absence of  $\pi$ -loops in  $45^\circ$  [100] tilt and twist grain boundaries junctions. The use of a  $\text{CeO}_2$  rather than a MgO seed layer can produce  $\pi$ -loops in the same junction configurations. The versatility of the biepitaxial technique has been recently used to obtain different types of grain boundaries. The advantage of placing junctions in arbitrary locations on the substrate without imposing any restrictions on the geometry, and the ease of obtaining different device configurations by suitably patterning the seed layer, make the biepitaxial technique competitive for the testing of new concept devices, such as those based on  $\pi$ -loops. Some simple examples of situations in which  $\pi$ -loops can be suitably produced in specific locations of a more complicated circuit have also been discussed.

## ACKNOWLEDGMENTS

This work has been partially supported by the projects PRA-INFM “HTS Devices” and SUD-INFM “Analisi non distruttive con correnti parassite tramite dispositivi superconduttori” and by a MURST COFIN98 program (Italy). The authors would like to thank Dr. E. Ilichev and A. Golubov for interesting discussions on the topic.

---

<sup>1</sup> L.B. Ioffe, V.B. Geshkenbein, M.V. Feigel'man, A.L. Fauchere and G. Blatter, *Nature* **398**, 679 (1999); G. Blatter, V. B. Geshkenbein and L. B. Ioffe, *Cond. Mat.* 9912163 (1999)

<sup>2</sup> L.N. Bulaevskii, V.V. Kuzii and A.A. Sobyenin, *JETP Lett.* **25**, 290 (1977)

<sup>3</sup> V.B. Geshkenbein, A.I. Larkin and A. Barone, *Phys. Rev. B* **36**, 235 (1986)

<sup>4</sup> C.C. Tsuei and J.R. Kirtley, to be published in *Review of Modern Physics* (1999); C.C. Tsuei, J.R. Kirtley, C.C. Chi, L.S. Yu-Jahnes, A. Gupta, T. Shaw, J.Z. Sun and M.B. Ketchen, *Phys. Rev. Lett.* **73**, 593 (1994); J.R. Kirtley, C.C. Tsuei, J.Z. Sun, C.C. Chi, L.S. Yu-Jahnes, A. Gupta, M. Rupp and M.B. Ketchen, *Nature* **373**, 225 (1995); D.A. Wollman, D.J. Van Harlingen, J. Giapintzakis, D.M. Ginsberg, *Phys. Rev. Lett.* **74**, 797 (1995); D.A. Wollman, D.J. Van Harlingen and A.J. Leggett, *Phys. Rev. Lett.* **73**, 1872 (1994)

<sup>5</sup> M. Sigrist and T.M. Rice, *J. Phys. Soc. Jap.* **61**, 4283 (1992)

<sup>6</sup> A.M. Zagoskin, *Cond. Mat.* 9903170 (1999)

- <sup>7</sup> R. Schulz, B. Chesca, B. Goetz, C.W. Schneider, A. Shmehl, H. Bielefeldt, H. Hilgenkamp and J. Mannhart, *Appl. Phys. Lett.* **76**, 912 (2000)
- <sup>8</sup> E. Il'ichev, V. Zakosarenko, R.P.J. Ijsselsteijn, H.E. Honig, V. Schultze, H.G. Meyer, M. Grajcar and R. Hlubina, *Phys. Rev. B* **60**, 3096 (1999)
- <sup>9</sup> E. Terzioglu and M.R. Beasley, *IEEE Trans. Appl. Supercond.* **8**, 48 (1998)
- <sup>10</sup> F. Tafuri, F. Miletto Granozio, F. Carillo, A. Di Chiara, K. Verbist and G. Van Tendeloo, *Phys. Rev. B* **59**, 11523 (1999)
- <sup>11</sup> K. Char, M.S. Colclough, S.M. Garrison, N. Newman and G. Zaharchuk, *Appl. Phys. Lett.* **59**, 773 (1991)
- <sup>12</sup> D. Dimos, P. Chaudari, J. Mannhart and F.K. LeGoues, *Phys. Rev. Lett.* **61**, 219 (1988)
- <sup>13</sup> R. W. Simon, J.F. Burch, K.P. Daly, W.D. Dozier, R. Hu, A.E. Lee, J.A. Luine, H.M. Manasevit, C.E. Platt, S.M. Schwarzbeck, D.St. John, M.S. Wire and M.J. Zani, in "Science and Technology of Thin Films Superconductors 2", R.D. McConnel and R. Noufi Eds. (Plenum, New York, 1990), p. 549
- <sup>14</sup> J. Mannhart, H. Hilgenkamp, B. Mayer, Ch. Gerber, J.R. Kirtley, K.A. Moler and M. Sigrist, *Phys. Rev. Lett.* **77**, 2782 (1996)
- <sup>15</sup> U. Scotti di Uccio, F. Lombardi, F. Ricci, E. Manzillo, F. Miletto Granozio, F. Carillo and F. Tafuri unpublished (2000)
- <sup>16</sup> K. Verbist, O. Lebedev, G. Van Tendeloo, F. Tafuri, F. Miletto Granozio and A. Di Chiara, *Appl. Phys. Lett.* **74**, 1024 (1999)
- <sup>17</sup> A. Barone and G. Paternoò, *Physics and Applications of the Josephson Effect*, (J. Wiley, New York, 1982)
- <sup>18</sup> J. Mannhart, R. Gross, K. Hipler, R.P. Huebner, C.C. Tsuei, D. Dimos and P. Chaudari, *Science* **245**, 839 (1989)
- <sup>19</sup> F. Tafuri, B. Nadgorny, S. Shokhor, M. Gurvitch, F. Lombardi, F. Carillo, A. Di Chiara and E. Sarnelli, *Phys. Rev. B* **57**, R14076 (1998)
- <sup>20</sup> F. Tafuri, S. Shokhor, B. Nadgorny, M. Gurvitch, F. Lombardi and A. Di Chiara, *Appl. Phys. Lett.* **71**, 125 (1997)
- <sup>21</sup> J.R. Kirtley *et al.*, *Appl. Phys. Lett.* **66**, 1138 (1995)
- <sup>22</sup> F. Tafuri and J.R. Kirtley, *cond-mat/0003106*.
- <sup>23</sup> D.B. Bailey, M. Sigrist and R.B. Laughlin, *Phys. Rev. B* **55**, 15239 (1997); M. Sigrist, *Progr. Theor. Physics* **99**, 899 (1998).
- <sup>24</sup> G. Testa, E. Sarnelli, F. Carillo and F. Tafuri, *Appl. Phys. Lett.* **75**, 3542 (1999)
- <sup>25</sup> A.H. Miklich, J. Clarke, M.S. Colclough, and K. Char, *Appl. Phys. Lett.* **60**, 1989 (1992)
- <sup>26</sup> Y. Tanaka and S. Kashiwaya, *Phys. Rev. B* **56**, 893 (1997)

FIG. 1. A schematic representation of the artificial grain boundary structure. The boundary is obtained at the interface between the [001] oriented YBCO film grown on the [110] MgO seed layer and the [103] YBCO film grown on the bare [110] STO substrate. In contrast with the  $45^\circ$  [001] tilt bicrystal junctions, in this case the order parameter orientations do not produce an additional  $\pi$  phase shift.

FIG. 2. The CeO<sub>2</sub> seed layer produces an artificial GB that can be seen as a result of two rotations: a 45° [100] tilt or twist followed by a 45° tilt around the c-axis of the (001) film. For this junction configuration a d-wave order parameter symmetry would produce  $\pi$ -loops.

FIG. 3. Current vs voltage (I-V) characteristics of the biepitaxial junction for temperature close to the critical temperature. In the inset the I-V curve at T = 4.2 K is shown.

FIG. 4. a) Scheme of the seed layer patterning, which allows the measurement on the same chip of the properties of a tilt junction and of junctions whose interface is tilted in plane of an angle  $\alpha = 30^\circ, 45^\circ$  and  $60^\circ$  with respect the a- or b-axis of the (001) YBCO thin film respectively. b) The I-V characteristics (measured at T = 4.2 K) of the microbridges reported in Fig. 4a.

FIG. 5. Magnetic-field dependence of the critical current of a [100] tilt biepitaxial dc-SQUID. The absolute maximum is observed for zero field. A double-period modulation is observed. The longer period modulation is the diffraction pattern due to the magnetic field sensed by a single junction, while the shorter period SQUID modulation is shown more clearly in the inset (a). In the inset (b) I-V curves are shown as a function of an externally applied magnetic field at T = 4.2 K. A typical Fraunhofer-like dependence is evident.

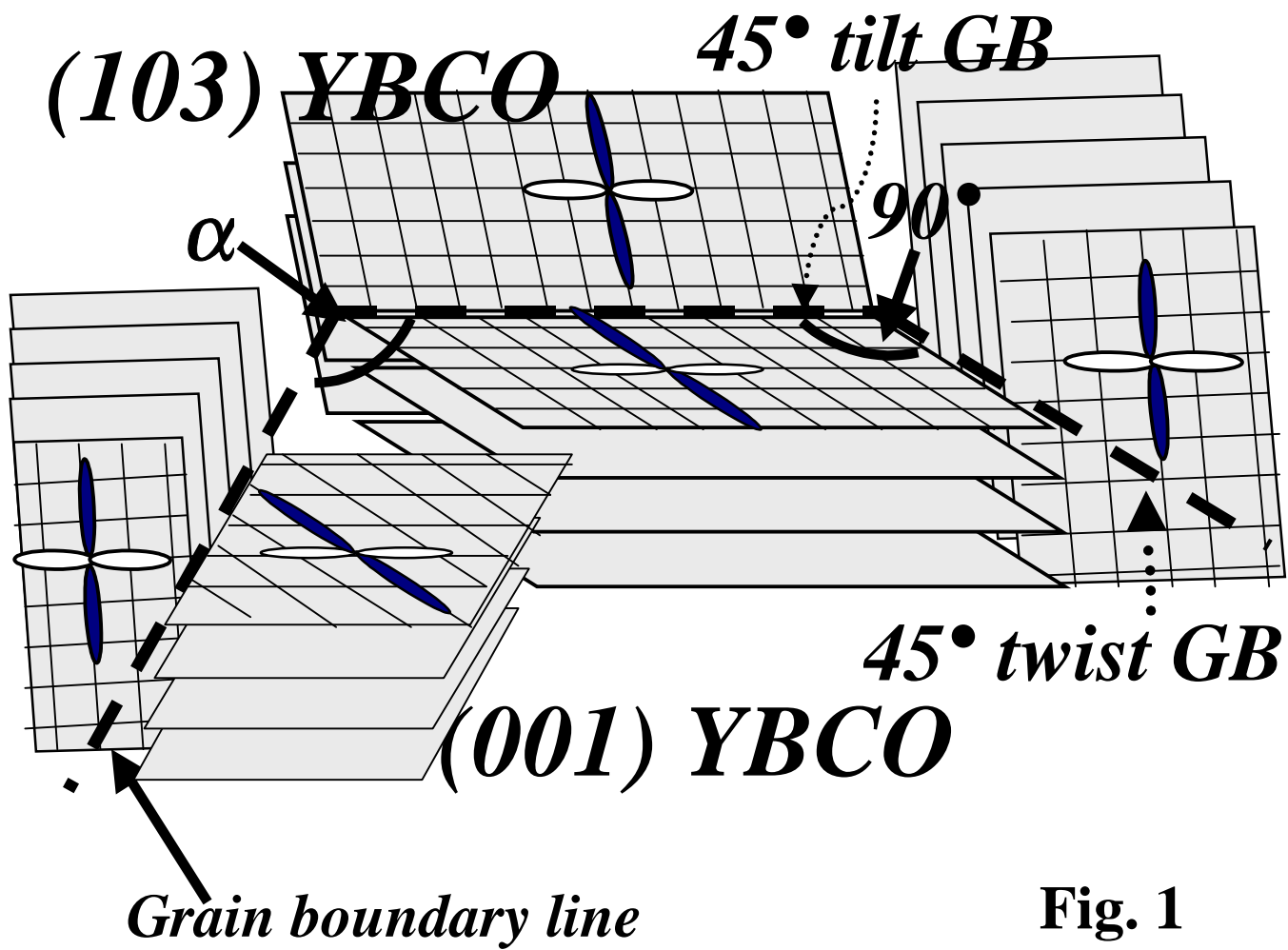
FIG. 6. Scanning SQUID microscope image of a  $200 \times 200 \mu\text{m}^2$  area along a grain boundary separating a (100) region from a (103) region of a thin YBCO biepitaxial film grown. The position of the grain boundary is indicated by the dashed line.

FIG. 7. Magnetic field dependence of the voltage of a [100] tilt biepitaxial dc-SQUID at 77 K for different values of the bias current.

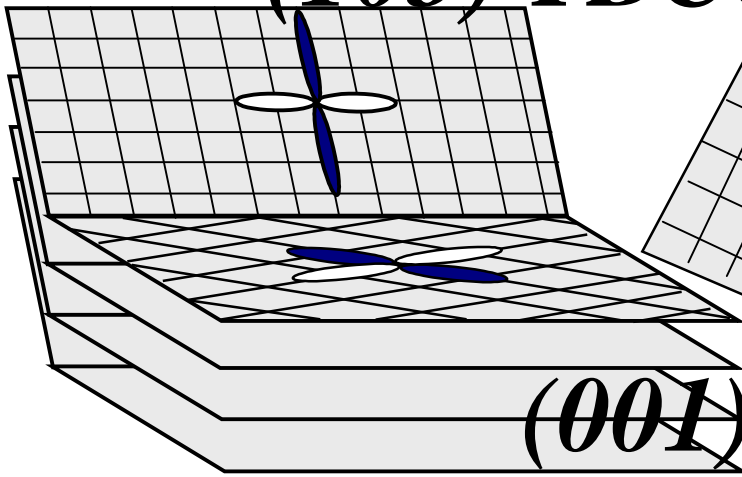
FIG. 8. Magnetic flux noise spectral densities of a [100] tilt biepitaxial SQUID at T=77 K and T=4.2 K. The SQUID, with an inductance L=13 pH, was modulated with a standard flux-locked-loop electronics. The right axis shows the energy resolution. Data at T = 4.2 K are compared with results on SQUIDS based on [001] tilt biepitaxial junctions from Ref. 25.

FIG. 9. a) 3-dimensional view of a SQUID based on 45° [100] tilt and twist GBs; no  $\pi$ -loops should occur. b) Top view of  $\pi$ -SQUID based on 45° [001] tilt GBs. c) 3-dimensional view of a  $\pi$ -SQUID based on GBs resulting from two rotations: a 45° [100] tilt or twist followed by a 45° [001] tilt

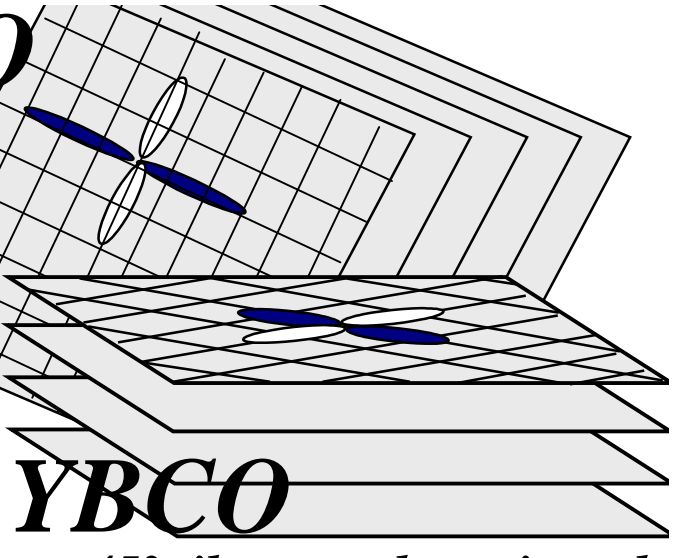
FIG. 10. Scheme of the qubit structure proposed in Ref.1 designed using the biepitaxial grain boundaries proposed in the paper. The double junctions of the original S-D-S' system can be also replaced by D'-D-D''.



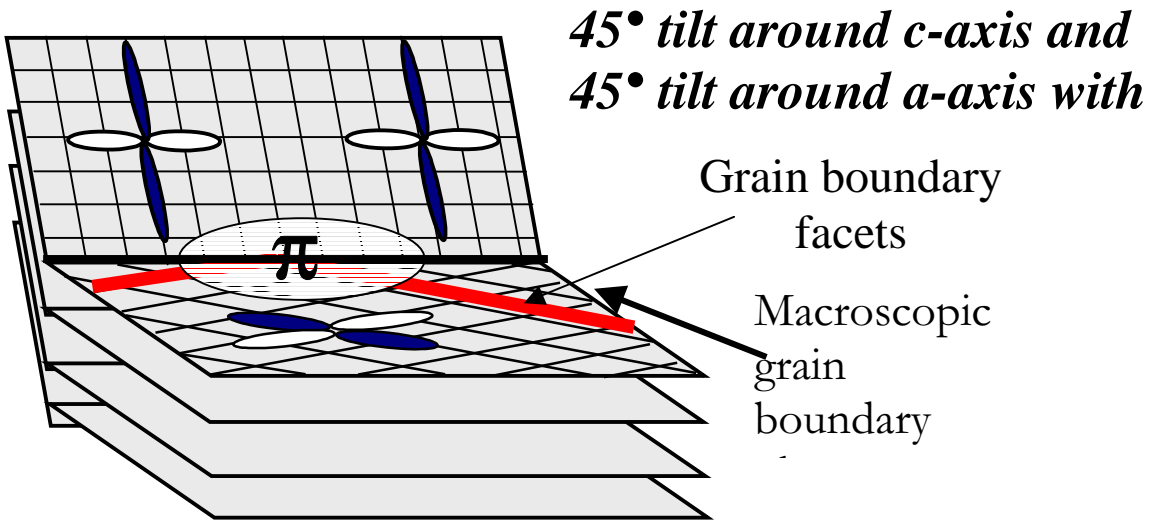
**(103) YBCO**



*45° tilt around c-axis and  
45° tilt around a-axis*



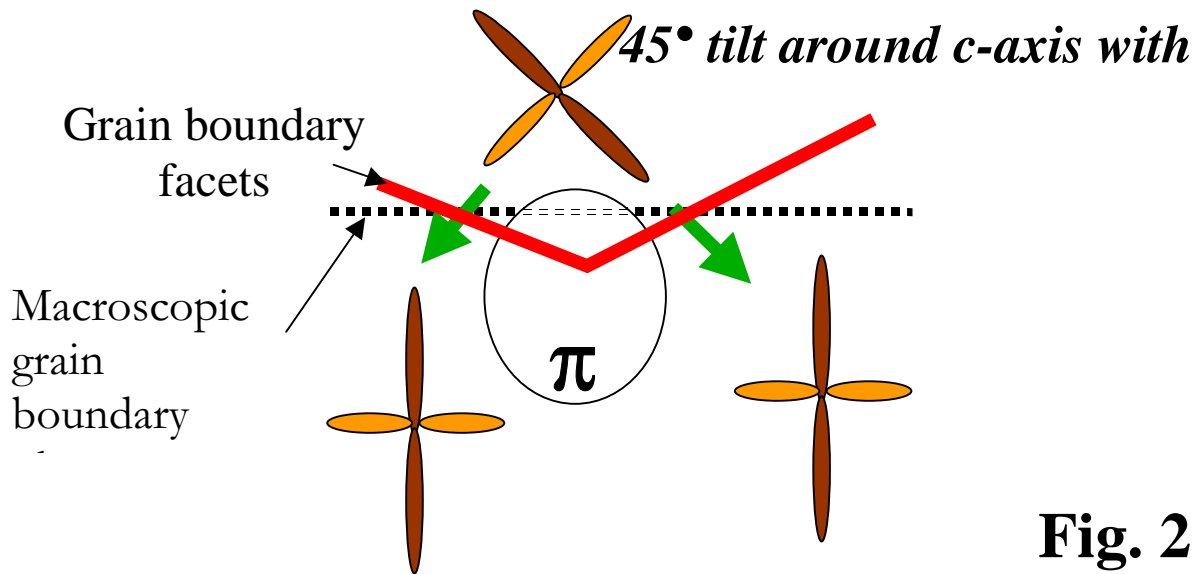
*45° tilt around c-axis and  
45° tilt around a-axis*



*45° tilt around c-axis and  
45° tilt around a-axis with*

Grain boundary  
facets

Macroscopic  
grain  
boundary



*45° tilt around c-axis with*

Grain boundary  
facets

Macroscopic  
grain  
boundary

**Fig. 2**

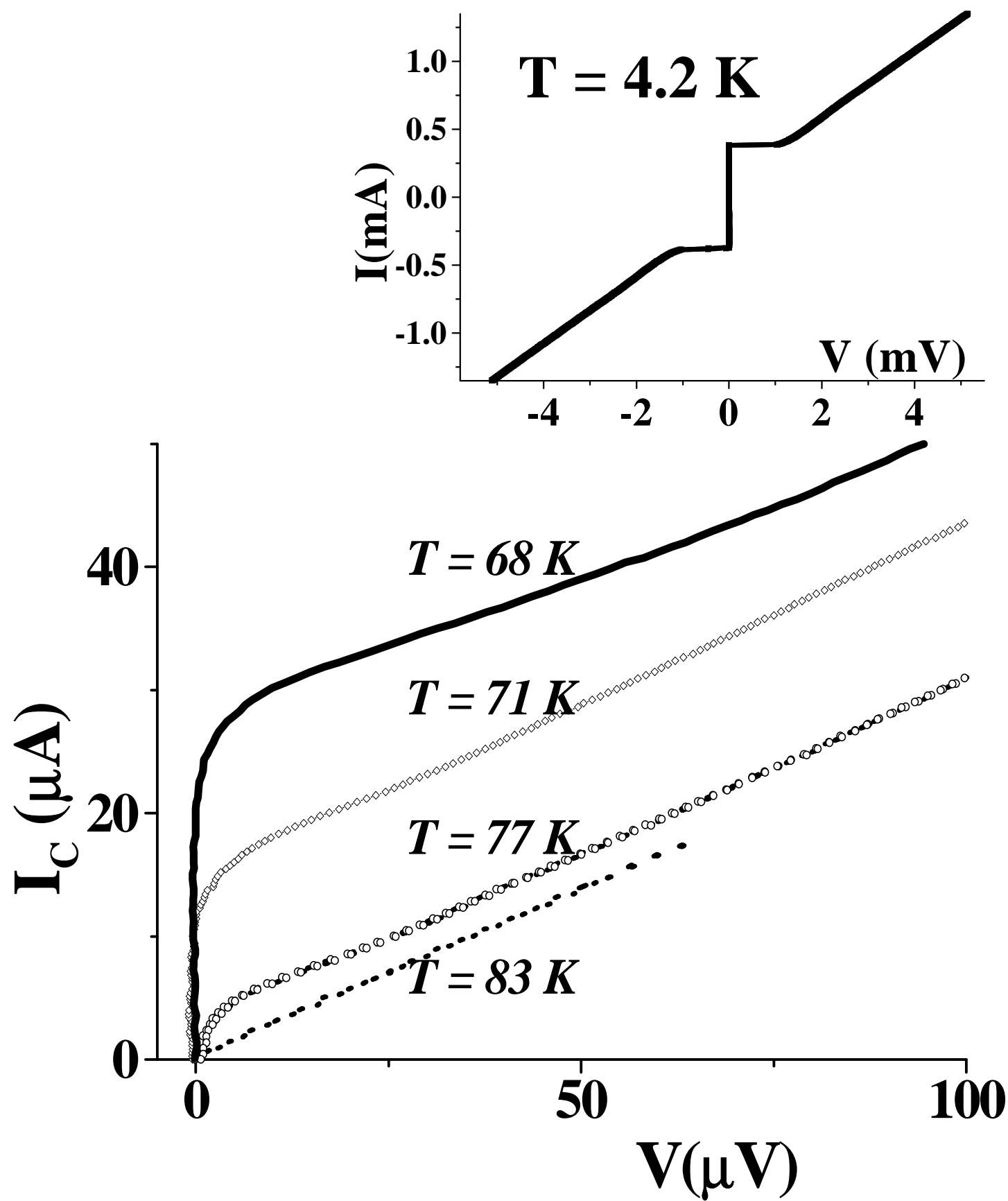
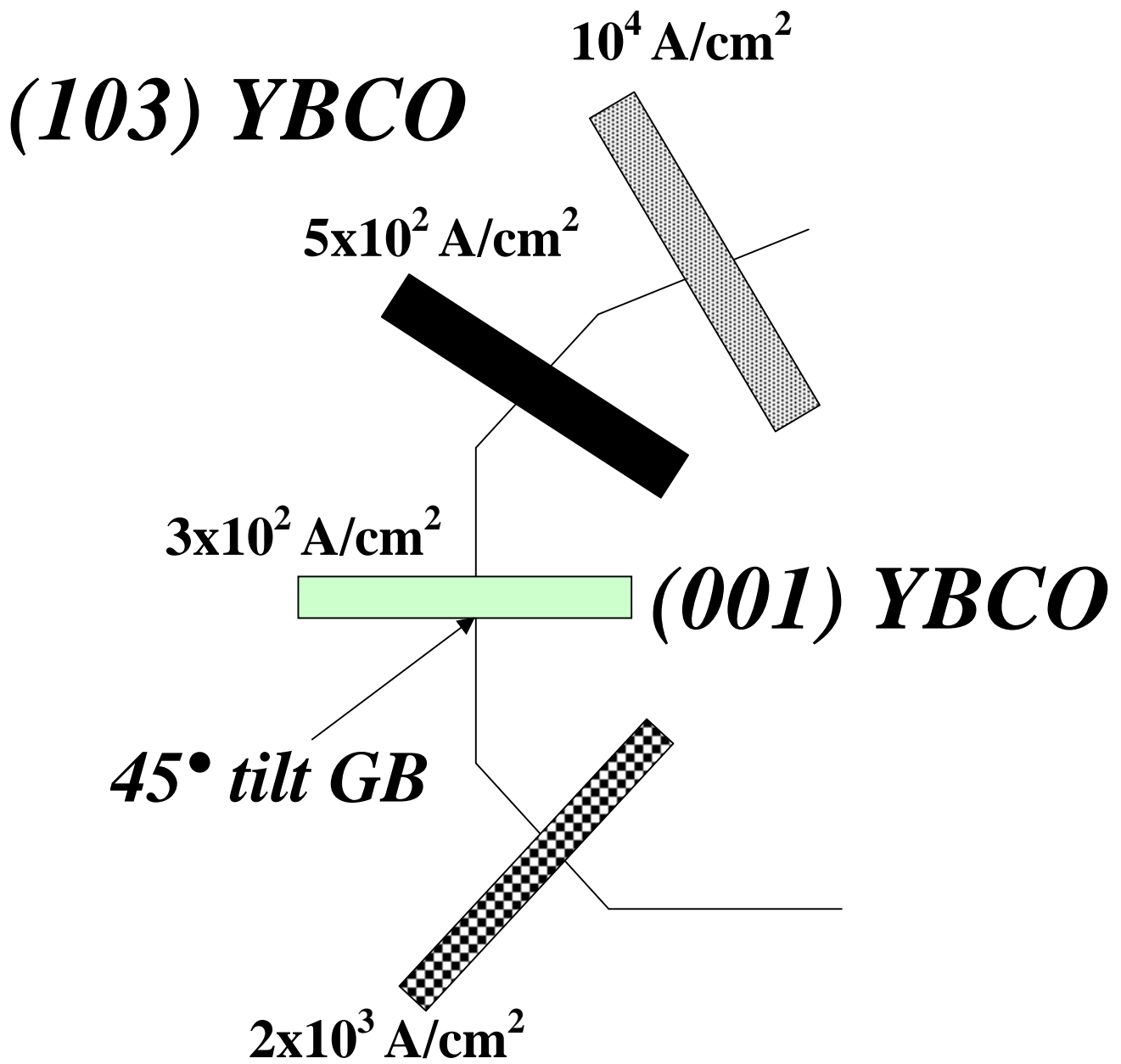
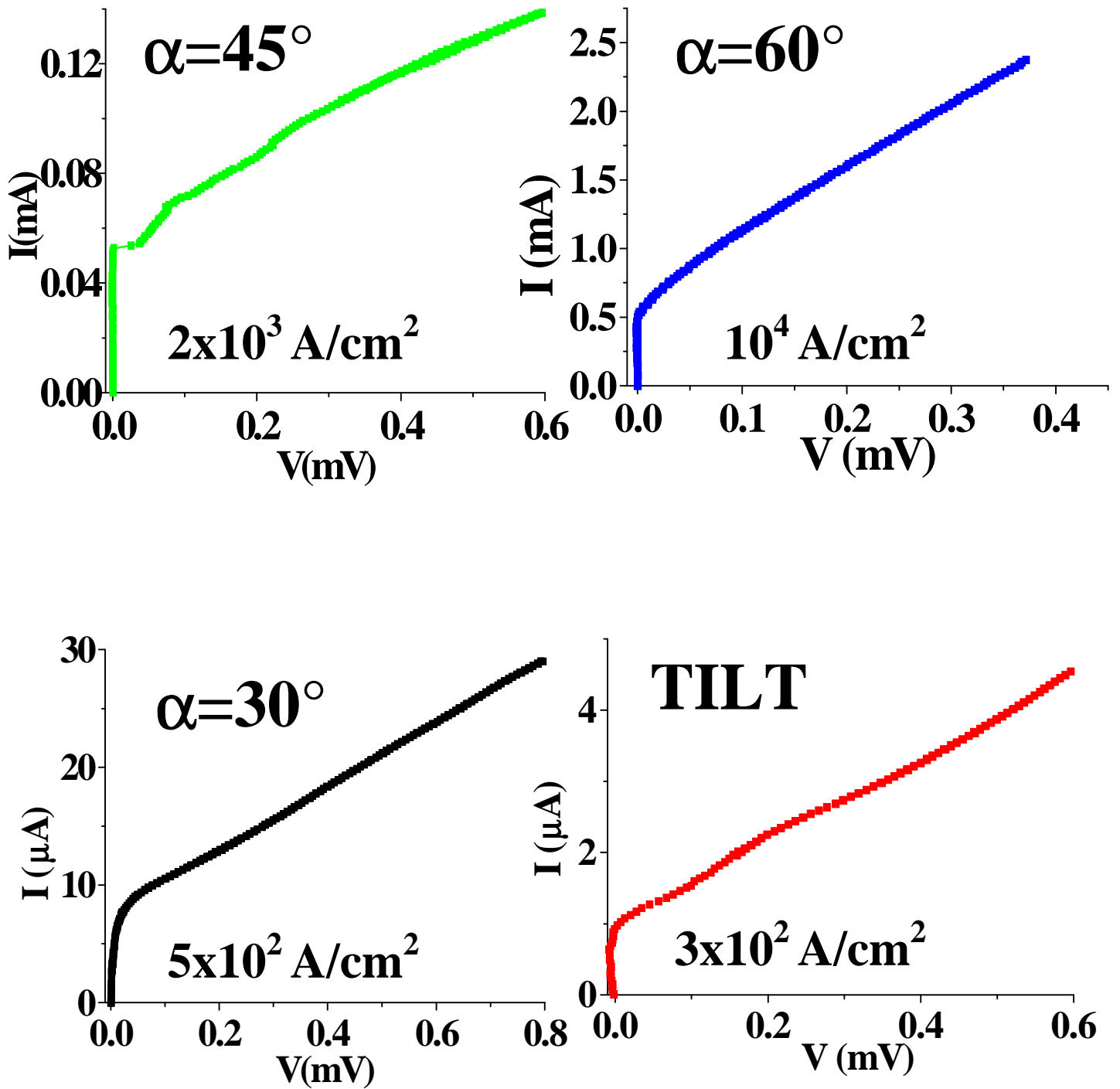


Fig. 3

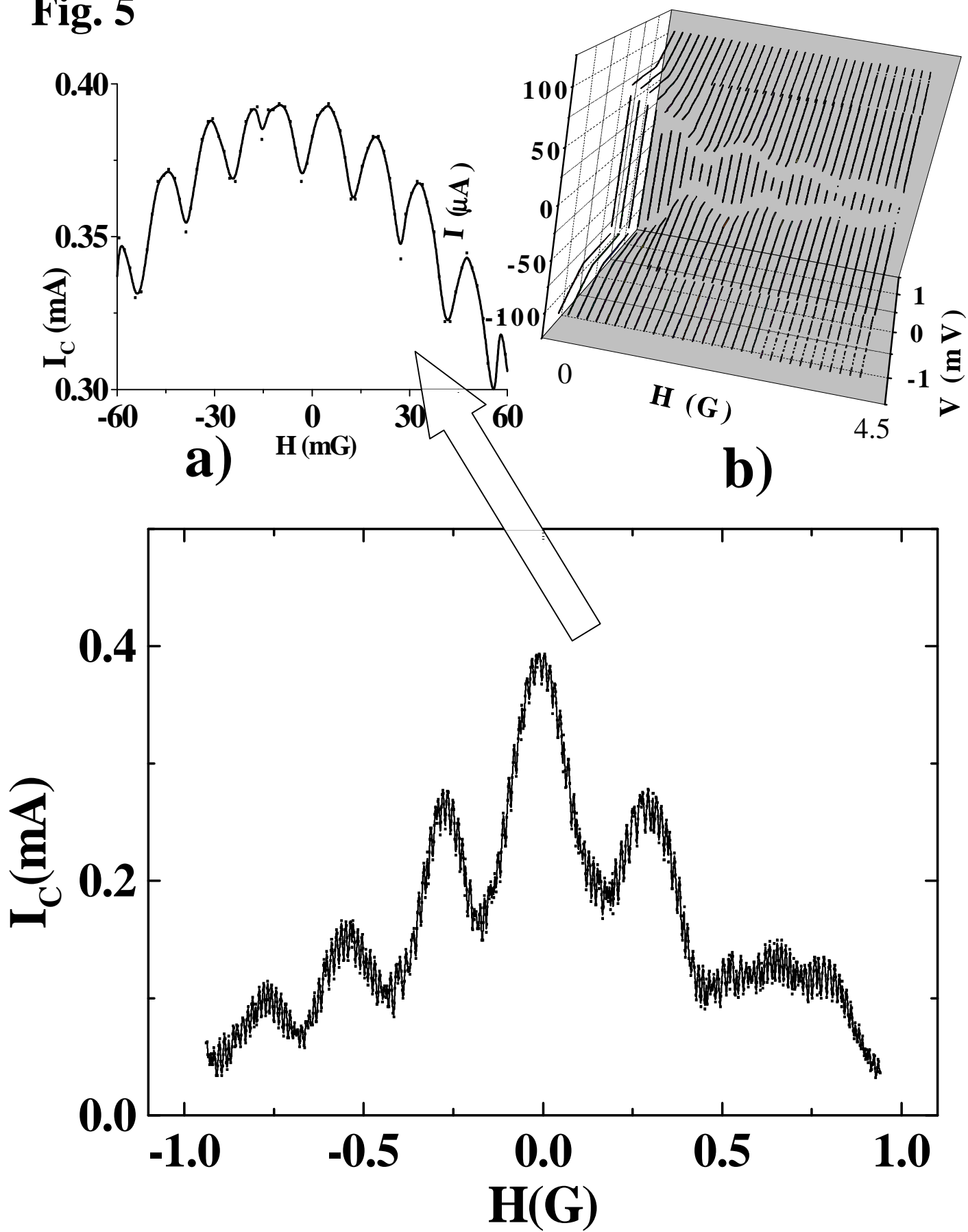


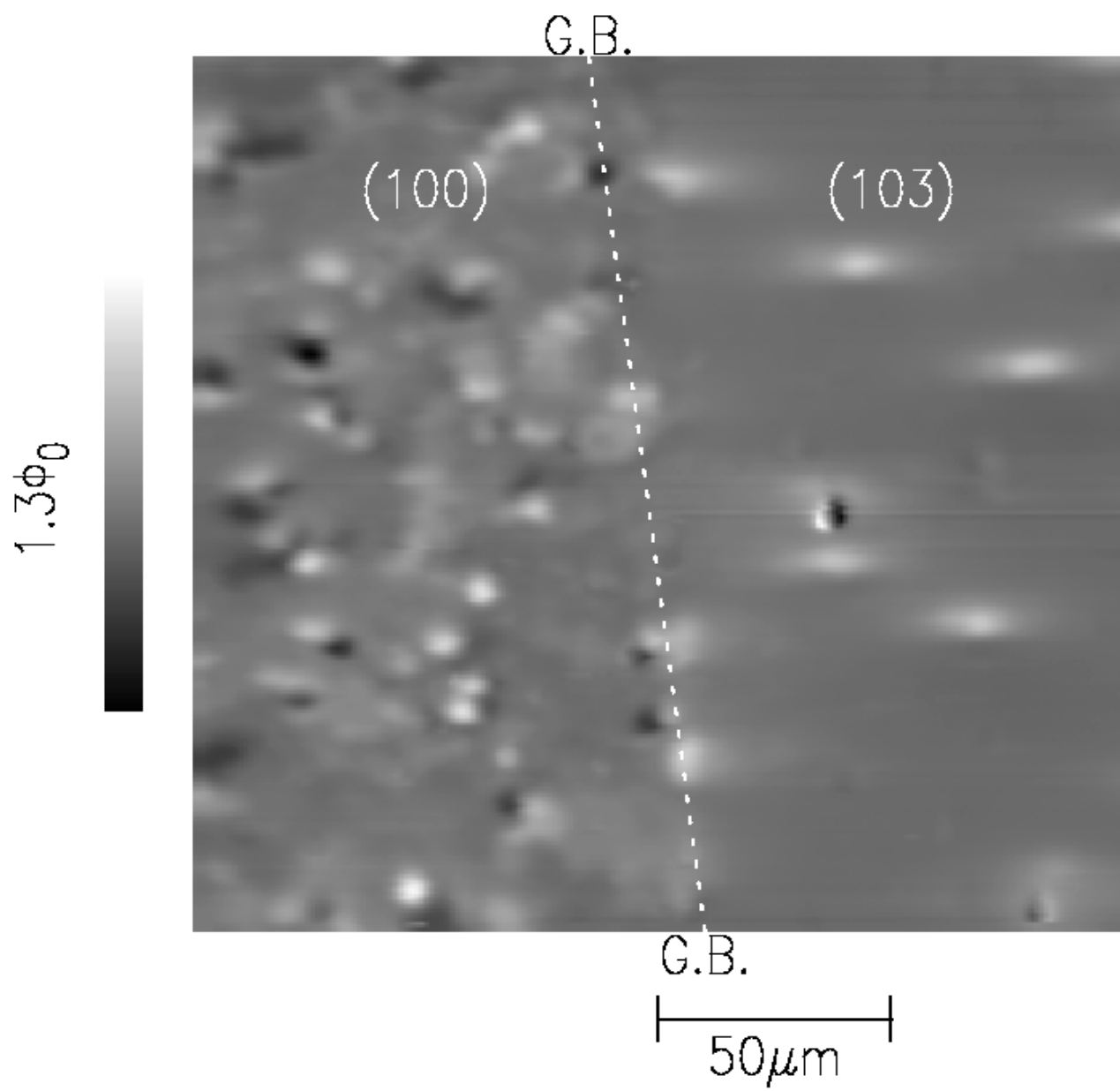
**Fig. 4a**

**Fig. 4b**

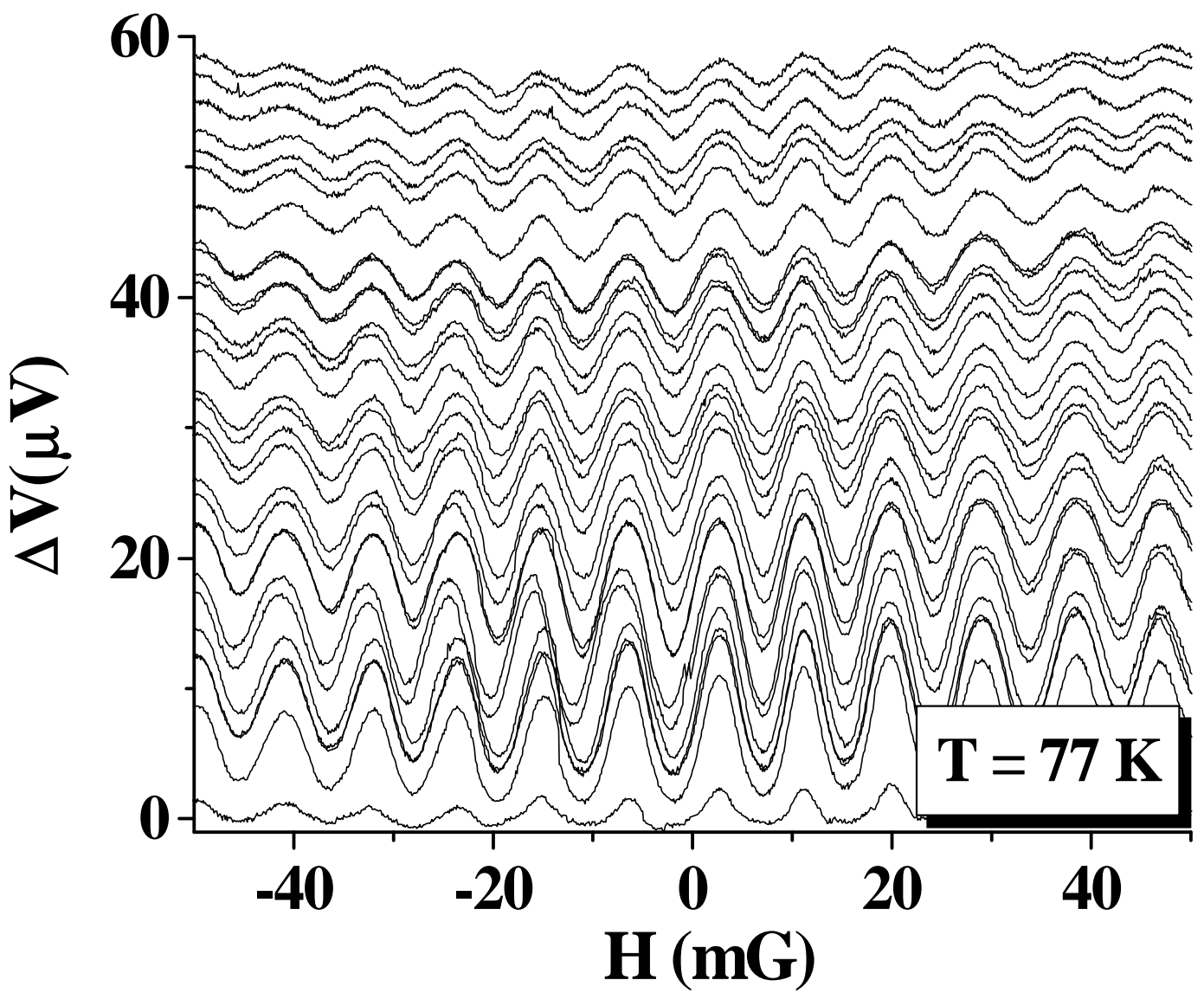


**Fig. 5**



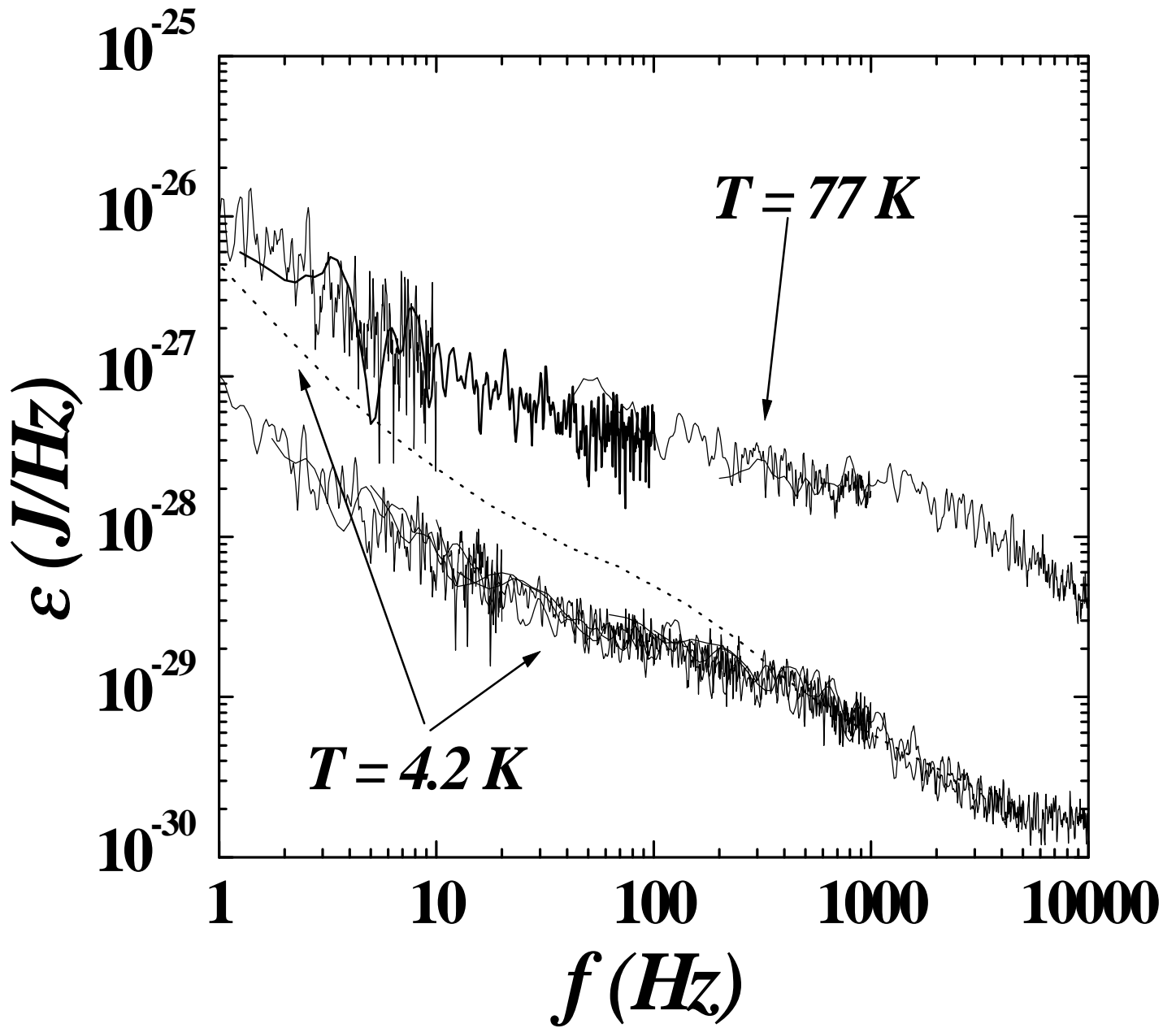


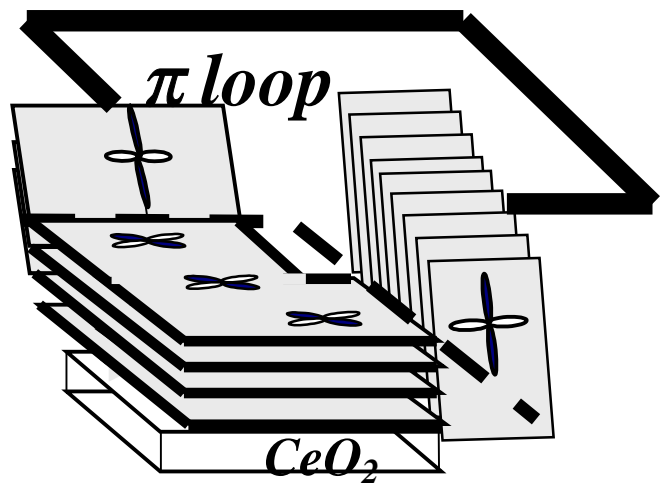
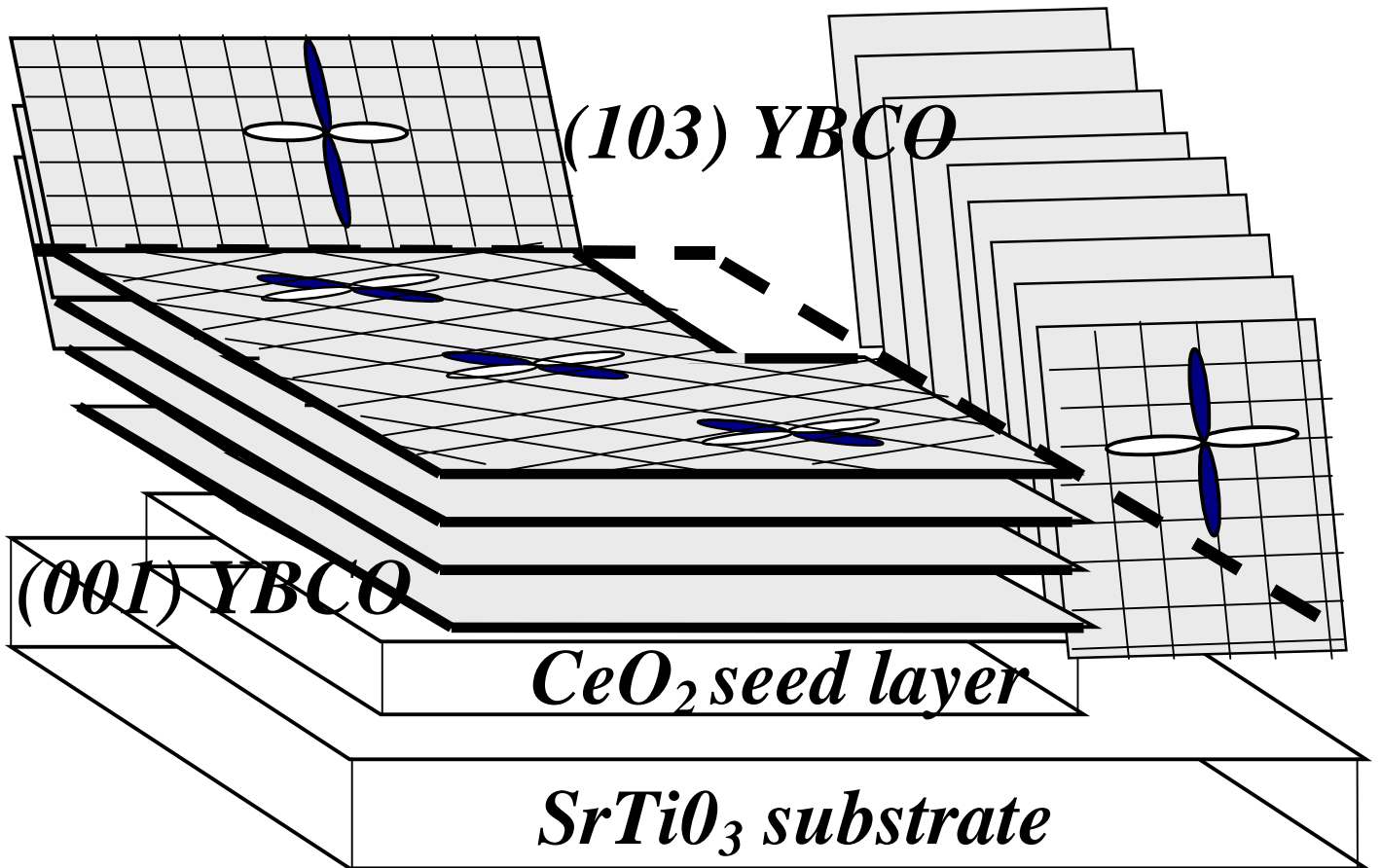
**Fig. 6**



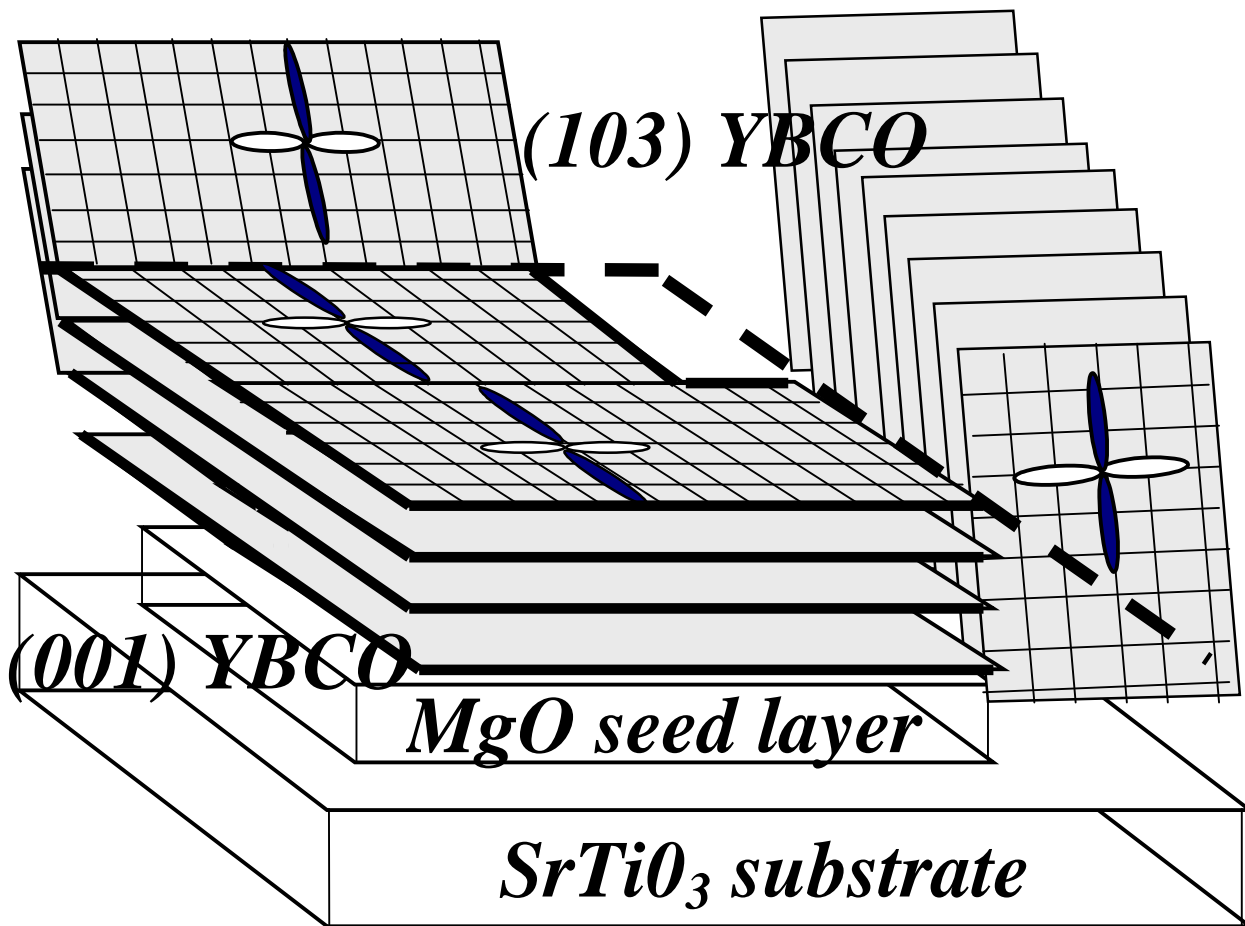
**Fig. 7**

**Fig. 8**



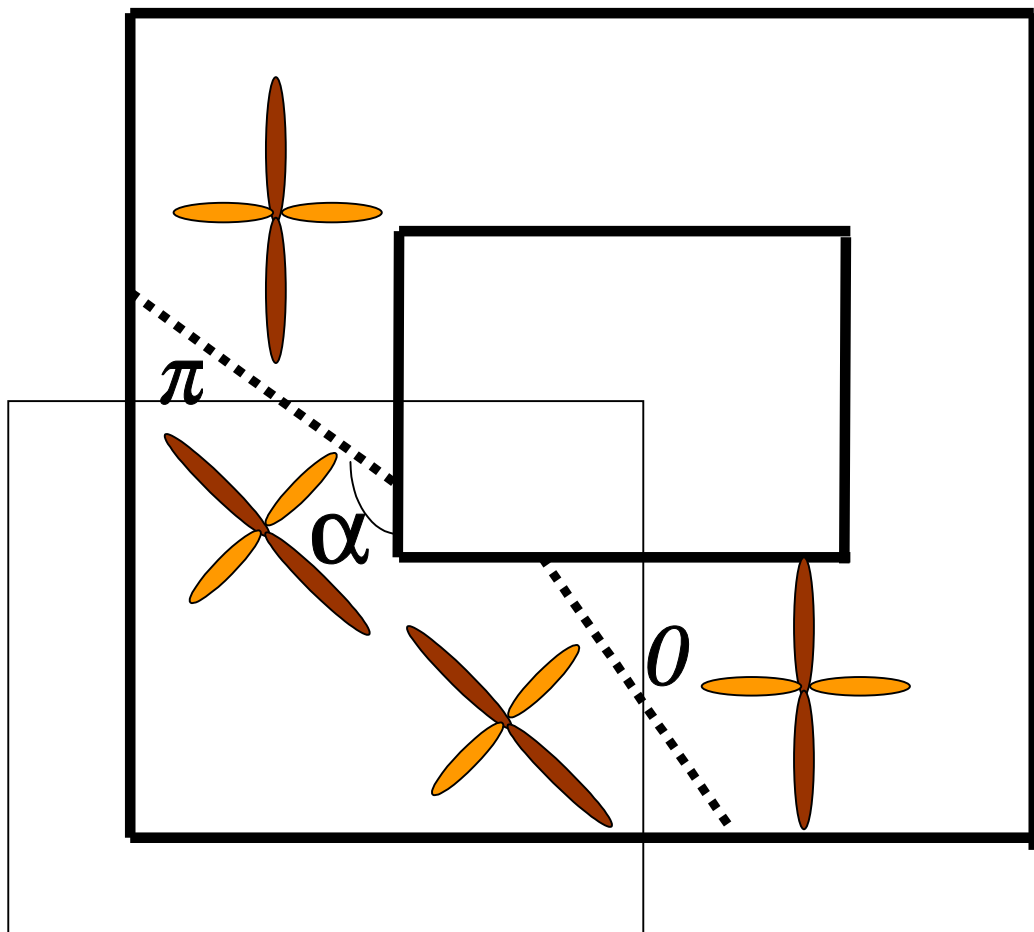
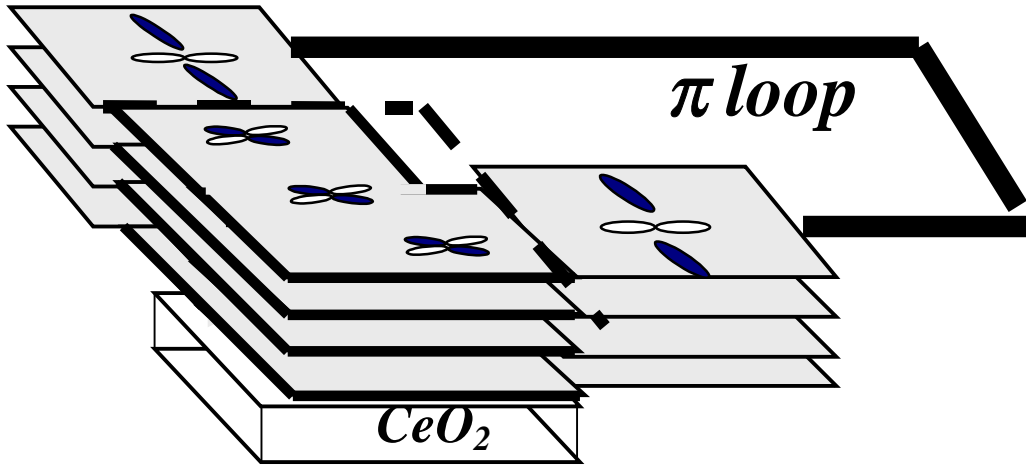


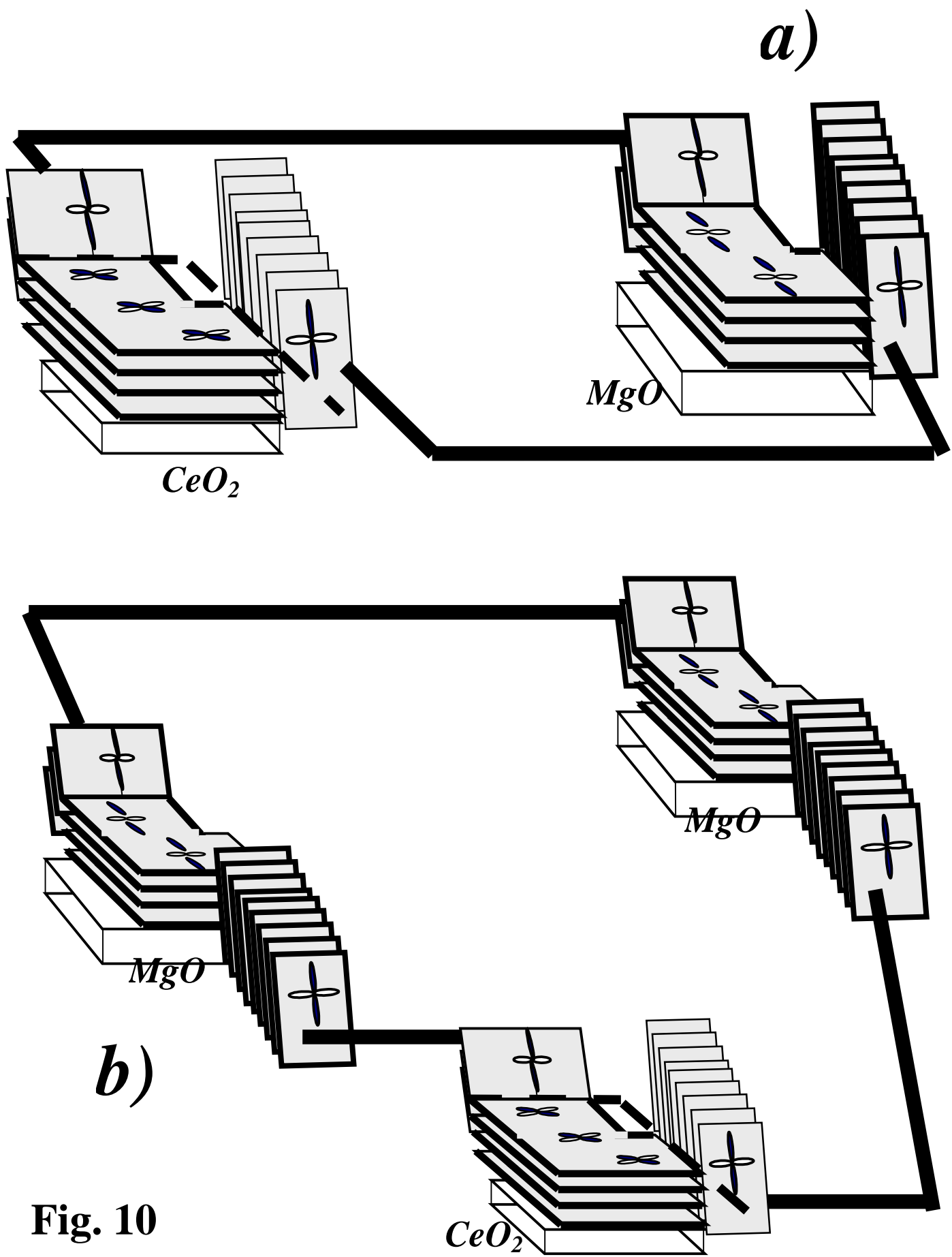
**Fig. 9a**



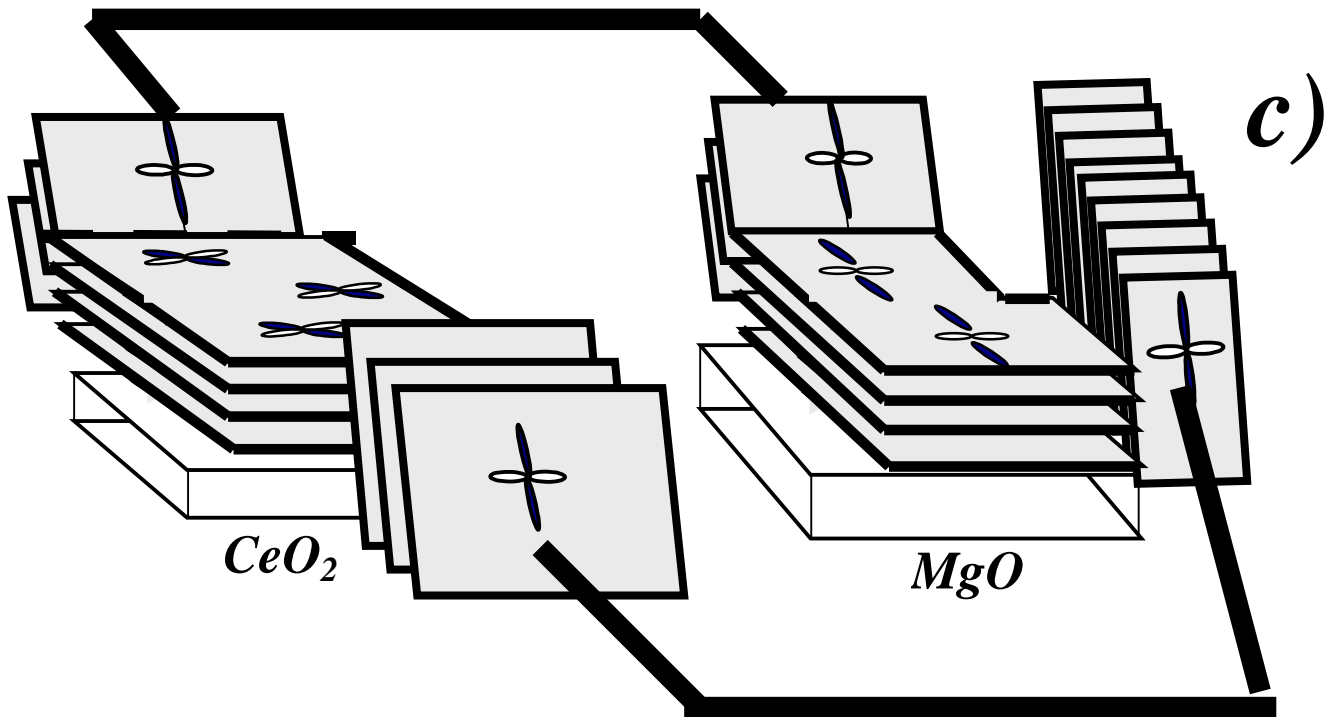
**Fig. 9b**

Fig. 9c





**Fig. 10**



**Fig. 10**